# Promoting angiogenesis and diabetic wound healing through delivery of protein transduction domain-BMP2 formulated nanoparticles with hydrogel

**Jae Wan Suh[1]\* [ID], Kyoung-Mi Lee[2]\*, Eun Ae Ko[2], Dong Suk Yoon[3], Kwang Hwan Park[2] [ID], Hyun Sil Kim[4], Jong In Yook[4], Nam Hee Kim[4] and Jin Woo Lee[2,5]**

## Abstract

Decreased angiogenesis contributes to delayed wound healing in diabetic patients. Recombinant human bone morphogenetic protein-2 (rhBMP2) has also been demonstrated to promote angiogenesis. However, the short half-lives of soluble growth factors, including rhBMP2, limit their use in wound-healing applications. To address this limitation, we propose a novel delivery model using a protein transduction domain (PTD) formulated in a lipid nanoparticle (LNP). We aimed to determine whether a gelatin hydrogel dressing loaded with LNP-formulated PTD-BMP2 (LNP-PTD-BMP2) could enhance the angiogenic function of BMP2 and improve diabetic wound healing. In vitro, compared to the control and rhBMP2, LNP-PTD-BMP2 induced greater tube formation in human umbilical vein endothelial cells and increased the cell recruitment capacity of HaCaT cells. We inflicted large, full-thickness back skin wounds on streptozotocin-induced diabetic mice and applied gelatin hydrogel (GH) cross-linked by microbial transglutaminase containing rhBMP2, LNP-PTD-BMP2, or a control to these wounds. Wounds treated with LNP-PTD-BMP2-loaded GH exhibited enhanced wound closure, increased re-epithelialization rates, and higher collagen deposition than those with other treatments. Moreover, LNP-PTD-BMP2-loaded GH treatment resulted in more CD31- and $\alpha$-SMA-positive cells, indicating greater neovascularization capacity than rhBMP2-loaded GH or GH treatments alone. Furthermore, in vivo near-infrared fluorescence revealed that LNP-PTD-BMP2 has a longer half-life than rhBMP2 and that BMP2 localizes around wounds. In conclusion, LNP-PTD-BMP2-loaded GH is a viable treatment option for diabetic wounds.

[1]Department of Orthopaedic Surgery, Dankook University College of Medicine, Cheonan, South Korea
[2]Department of Orthopaedic Surgery, Yonsei University College of Medicine, Seoul, South Korea
[3]Department of Biomedical Science, Hwasung Medi-Science University, Hwaseong-Si, Gyeonggi-Do, South Korea
[4]Department of Oral Pathology, Oral Cancer Research Institute, Yonsei University College of Dentistry, Seoul, South Korea
[5]Brain Korea 21 PLUS Project for Medical Science, Yonsei University College of Medicine, Seoul, South Korea

\*These authors contributed equally to this work.

**Corresponding authors:**
Nam Hee Kim, Department of Oral Pathology, Oral Cancer Research Institute, Yonsei University College of Dentistry, 50-1, Yonsei-ro, Seodaemun-gu, Seoul 03722, South Korea.
Email: migo77@yuhs.ac

Jin Woo Lee, Department of Orthopaedic Surgery, Yonsei University College of Medicine, 50-1, Yonsei-ro, Seodaemun-gu, Seoul 03722, South Korea.
Email: ljwos@yuhs.ac

## Introduction

Diabetes mellitus is a chronic metabolic disorder affecting millions of people worldwide.[1,2] Diabetic foot ulceration, one of the most common complications of diabetes, is associated with delayed wound healing.[3,4] Wound healing involves a well-coordinated sequence of cellular and bio-molecular events, including inflammation, cell migration and proliferation, and tissue remodeling.[2,5] However, diabetic wounds exhibit abnormal chemokine production and inflammatory responses, decreased growth factor levels, and reduced angiogenic activity.[4,6–8] Previous research has explored the efficacy of advanced treatments involving stem cells, chemokines, growth factors, skin substitutes, and gene therapy for improving diabetic wound healing. Nonetheless, their efficacy remains low, highlighting the need for more effective treatment methods.[9]

Insufficient angiogenesis results in limited recruitment of inflammatory cells and a reduced supply of oxygen and nutrients.[6] Impaired recruitment and migration of cells to wound sites also decrease the chemokine production crucial for wound repair.[2,6,7] Thus, enhancing angiogenesis is one of the main strategies for treating diabetic wounds.[9,10] Although growth factor treatments can improve angiogenesis, their short half-lives and adverse effects limit their success.[6,7,9]

Recombinant human bone morphogenetic protein-2 (rhBMP2) has received Food and Drug Administration (FDA) approval for bone regeneration.[11,12] Moreover, numerous studies have demonstrated the critical role of BMP2 in physiological development and vascular homeostasis,[13] including angiogenesis.[14–16] BMP signaling regulates mesoderm formation, vasculogenesis, sprouting angiogenesis, arteriovenous differentiation, endothelial barrier function, and endothelial-to-mesenchymal transition.[13,17] Furthermore, BMP signaling influences endothelial cell (EC) migration, proliferation, and network formation.[13] During sprouting angiogenesis, BMP signaling promotes vascular morphogenesis by controlling vascular activation and maturation.[13] BMP2 also induces in vitro proliferation of human pulmonary artery and aortic ECs, increases migratory efficiency, and promotes tube formation in human dermal microvascular ECs, as well as human aortic and umbilical vein ECs.[13,15,18–21]

The angiogenic potential of BMP2 led us to hypothesize that it could improve diabetic wound healing. However, few studies have explored the association between BMP2 and wound healing. Since BMP2 can influence bone formation, potential side effects may include ectopic ossification or vascular calcification.[22,23] Nonetheless, the activation of BMP signaling plays a role in stem cell recruitment to wound sites and wound healing acceleration.[24]

The short half-life of rhBMP2 necessitates its administration at high dosages to be effective. Research aiming to overcome this limitation has been actively conducted. In a previous study, a recombinant protein transduction domain (PTD)-fusion polypeptide was delivered intracellularly across the membrane without any specific receptor.[25,26] After transduction, the PTD-fusion polypeptide refolded, was post-translationally cleaved, and secreted in its active form.[11,26,27] We reported PTD-BMP2 as a prodrug of BMP2 using this strategy.[11] It demonstrated improved functionality in vivo at a lower dose than rhBMP2.[11] Moreover, to overcome the size limitation imposed by endosomal cellular delivery, we previously developed PTD-BMP7 formulated in micelles as lipid nanoparticles (LNPs).[28,29] The micelle enhanced endosomal transduction of PTD-BMP7, and micellized PTD-BMP7 was successfully processed and secreted as active BMP7.[28,29]

We hypothesize that a newly designed PTD-BMP2 formulated in micelles could induce intracellular transduction in wounds and secrete active BMP2, leading to enhanced angiogenesis, improved cell recruitment, and a more effective reparative process for wound healing (Scheme 1). Therefore, this study aimed to investigate whether LNP-formulated PTD-BMP2 (LNP-PTD-BMP2) could successfully enter a diabetic wound when applied via a gelatin hydrogel (GH) dressing and whether the angiogenic function of BMP2 could improve diabetic wound healing.

## Materials and methods

### Preparation of LNP-PTD-BMP2

Recombinant PTD-BMP2 was synthesized as previously described.[11] The PTD-fusion BMP2 polypeptide was amplified using pRSET (Invitrogen, Waltham, MA, USA), a bacterial expression vector containing an Xpress epitope and a His tag. The precursor cDNA of BMP2 was amplified from the cDNA of Saos-2 osteosarcoma cells using polymerase chain reaction. The TAT sequences (RKKRRQRRR) for the PTD domain were inserted adjacent to the epitope, and the precursor cDNAs of BMP2 were cloned into a TAT-expression cassette. Following the transformation of BL21 competent cells and IPTG induction, inclusion bodies were obtained from the insoluble fraction using 1% Triton X-100 buffer. The insoluble fraction was solubilized with an 8 M urea solution, and the recombinant protein was purified using Ni-Ti beads and imidazole elution. Buffer shock was then employed to imbue high surface energy ($\Delta G$) properties. Denatured polypeptides were micellized with filtered 0.1% egg lecithin (BOC Sciences, Shirley, NY, USA) via bath sonication.[28,29]

### Preparation of LNP-PTD-BMP2-loaded GH

GH was synthesized as previously described.[30,31] Gelatin gels were prepared by cross-linking gelatin using microbial transglutaminase (mTG). TI transglutaminase formula (Modernist Pantry) was dissolved in phosphate-buffered
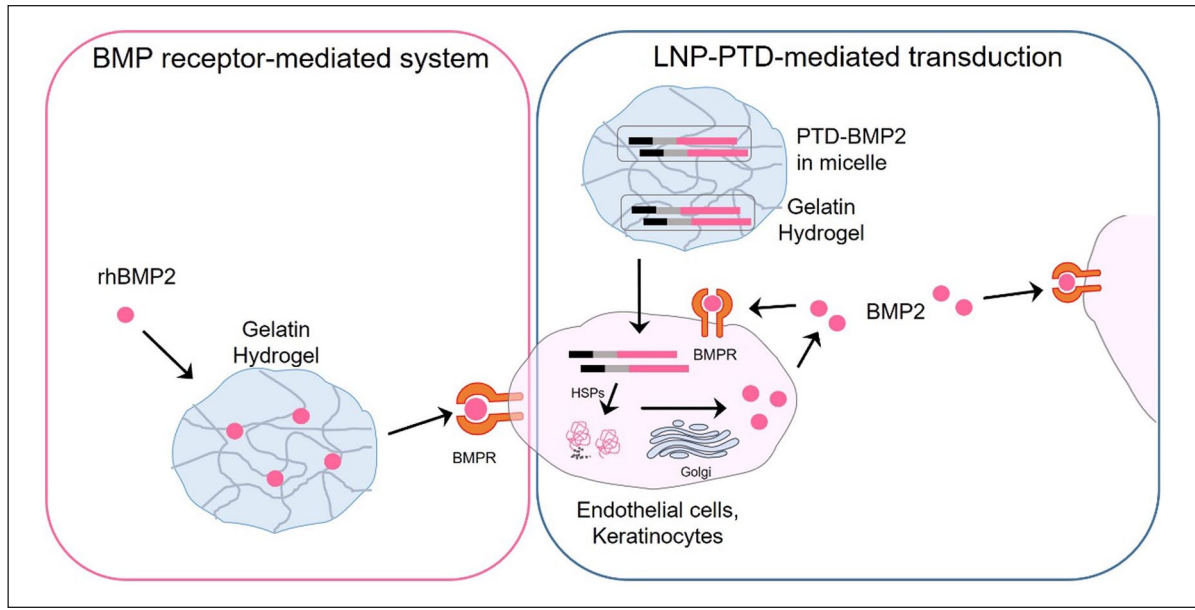
**Scheme 1.** Schematic illustration of the approaches used in this study: The back wound of a streptozotocin-induced diabetic mouse was treated with either rhBMP2- or LNP-PTD-BMP2-loaded gelatin hydrogel. Following intracellular transduction of micellized PTD-BMP2 and subsequent processing, active BMP2 was secreted, leading to autocrine and paracrine action.

saline (PBS) to obtain a 10% (wt, weight ratio) mTG solution. Subsequently, gelatin (Sigma-Aldrich, St. Louis, MO, USA) was added at 5.5% (w/v%: weight/total solution volume) in PBS. GHs were prepared by mixing the appropriate volume of the 10% mTG solution with 5.5% gelatin, according to the experimental requirements. As previously described, 4.4% GH at $200\,\mu L/cm^2$ was used.[31] The GH, mTG solution, and LNP-PTD-BMP2 were mixed at room temperature.

### In vitro cell migration study

In vitro cell migration study was assessed using a scratch wound assay as previously described.[32,33] HaCaT cells were seeded at a density of $2 \times 10^5$ cells/mL into 6-well plates and incubated at 37°C under 5% $CO_2$. When the cells reached 80%–90% confluency, they were scratched using $200$-$\mu L$ micropipette tips. Floating cells were immediately removed by washing with PBS, and 1.5 mL of culture medium was added. Because the LNP-PTD-BMP2 was purified in an *E. coli* system, we used *E. coli*-derived rhBMP2 (Daewoong Pharmaceutical Co., Ltd., Seoul, Korea). rhBMP2 and LNP-PTD-BMP2 were added at concentrations of 100 ng/mL each. After 48 h of cell culture, images were captured using a digital camera (Nikon, Tokyo, Japan) coupled to an optical microscope (Nikon TMS). Quantification of the percentage of wound closure between 0 and 48 h was assessed using ImageJ software (Ver. 1.48, Aspire Software International, Leesburg, VA, USA). All experiments were repeated at least three times.

### HaCaT cell proliferation assay with LNP-PTD-BMP2

The proliferation of HaCaT cells by LNP-PTD-BMP2 was evaluated using a water-soluble tetrazolium salt (WST) assay (EZ-Cytox Kit, Daeil Lab Service, Seoul, Korea). First, HaCaT cells were seeded in 12-well plates at $1 \times 10^4$ cells/mL and incubated with 100 ng/mL LNP-PTD-BMP2 for 24, 72, and 120 h at 37°C and 5% $CO_2$. Then, $10\,\mu L$ of EZ-Cytox solution was added to each well, and the cells were incubated at 37°C for 3 h. The absorbance was measured at 450 nm. All samples were tested in triplicate.

### In vitro angiogenesis study via tube formation assay

EC migration and capillary tube formation assays were used to assess angiogenesis in vitro.[34,35] Human umbilical vein endothelial cell (HUVEC) capillary tube formation assays were performed to assess LNP-PTD-BMP2-induced angiogenesis in vitro.[35]

Primary HUVECs (Lonza, Basel, Switzerland) were cultured in EC growth medium-2 (EBM-2, Lonza) supplemented with 10% fetal bovine serum (FBS, Gibco-Invitrogen), 100 units/mL penicillin G, and $100\,\mu g/mL$ streptomycin at 37°C under 5% $CO_2$/95% air. All cells used in experiments underwent fewer than eight passages after resuscitation.[35] Additionally, 500 ng of LNP-PTD-BMP2 was added to the HUVEC culture medium and allowed to incubate overnight. The insoluble fractions of

cells were used for western blotting to detect transduced recombinant protein in cells.

The tube-like structures formed by HUVECs on Matrigel with reduced quantities of growth factors were analyzed as previously described.[36–38] Briefly, 96-well culture plates were coated with Matrigel (50 μL/well) and incubated for 30 min at 37°C. After HUVECs were cultured in EBM-2 containing 1% FBS, they were plated onto a layer of Matrigel at a density of $2 \times 10^4$ cells/well. Following a 2-h incubation at 37°C, the cells were treated with either $H_2O_2$ (200 nM), rhBMP2 (100 ng) with $H_2O_2$ (200 nM), or LNP-PTD-BMP2 (100 ng) with $H_2O_2$ (200 nM). Each well was analyzed at 1-h intervals for up to 6 h. Tube formation was observed using an inverted phase-contrast microscope, and the number of nodes and tubes were quantified.

## In vivo BMP2 release test and diabetic wound healing study

*Preparation of streptozotocin (STZ)-induced diabetic mouse model.* ICR mice (male, 7 weeks old) were procured from Orient Bio (Seoul, Korea) and housed in wire cages. The temperature and humidity of the cages were maintained at 20–22°C and 40–50%, respectively, throughout the experiment. Type I diabetes was induced in all mice by intraperitoneally injecting STZ (Sigma-Aldrich) dissolved in 0.05 M citrate buffer, pH 4.5, at a dosage of 200 mg/kg body weight. One week later, a diabetic phenotype was confirmed using a OneTouch Select meter (Johnson & Johnson, UK) when the fasted blood glucose level exceeded 300 mg/dL. The animal studies were conducted in compliance with the guidelines set by the Institutional Animal Care and Use Committee (IACUC) and authorized by the Yonsei University College of Medicine (Permit No. 2018-0325).

*Diabetic wound treatment with rhBMP2 or LNP-PTD-BMP2-loaded GH dressings.* Mice (male, 9 weeks old) were anesthetized through intraperitoneal injection of Zoletile (30 mg/kg body weight) and Rompun (10 mg/kg body weight). The hair on the mice's backs were shaved and wiped with 70% ethanol. Full-thickness skin wounds (10 mm in diameter) were created on the backs of diabetic mice. Silicone rings were sutured around each wound to prevent wound contraction.[2,39]

The groups for evaluating the efficacy of LNP-PTD-BMP2-loaded GHs were as follows: Defect (untreated group), GH (a group treated with GH only), rhBMP2 (a group treated with rhBMP2-loaded GH), and LNP-PTD-BMP2 (a group treated with LNP-PTD-BMP2-loaded GH). The wounds were treated once after surgery by filling them with GH, rhBMP2-loaded GH, or LNP-PTD-BMP2-loaded GHs (5 mice/group) using a pipette.

Subsequently, all wounds were covered with Vaseline gauze (Covidien, USA), which served as a moist dressing to minimize GH dehydration. The wound dressing and gauze were changed twice a week. The concentration of rhBMP2 used was 100 ng/cm². The optimized concentrations of LNP-PTD-BMP2 used were 0, 25, 100, and 400 ng/cm².

*Measurement of BMP2 release.* Indocyanine green (ICG)-labeled rhBMP2- or LNP-PTD-BMP2-loaded GH was applied to the wound site. After dressing the wound, near-infrared fluorescent images were captured in vivo at 0, 1, 3, 5, and 7 days using an animal optical imaging system (IVIS, Caliper Life Sciences, Waltham, MA, USA). During imaging, the mice were anesthetized using isoflurane inhalation. The excitation and emission wavelengths of ICG were 780 and 831 nm, respectively. The fluorescence signal (p/s/cm²) from each mouse was measured using Living Image software (version 2.50, Xenogen, Alameda, CA, USA). All tests were conducted with five mice.

*Measurement of wound closure.* Photographs of the wounds were captured using a digital camera (Nikon, Japan) at days 0, 3, 7, 10, and 14. To evaluate the degree of wound closure, the remaining wound area was measured using ImageJ software. The regenerated wound area on the specified day $(A_t)$ relative to the initial wound area on day zero $(A_0)$ (%) was calculated as $[(A_0 - A_t)/A_0] \times 100$.[40]

*Histological analysis of regenerative tissues.* At the time of sacrifice, perilesional skin samples were collected and fixed in a 10% formalin solution. The skin samples were stained with hematoxylin and eosin (H&E) and Masson's trichrome (MT). The wound area was digitally analyzed using ImageJ software. The distance between the regenerated keratinocyte cell layers was measured on both ends of the wound. The re-epithelialization rate was determined by comparing the measured distances with those in the initial wound images of MT-stained histological sections.

Collagen deposition in regenerated skin tissue at 14 days was measured by counting the pixels in MT-positive blue areas of granulation and assessing the staining intensity, using ImageJ software for quantitative analysis. Von Kossa staining was employed to evaluate calcium deposition in regenerated perilesional skin tissue. A total of five mice per group were analyzed to determine the histology of the regenerated tissues.

*Immunofluorescence.* The central wound area was sectioned for immunofluorescence analysis. The sections were deparaffinized, rehydrated, washed twice with PBS, and then incubated with $H_2O_2$ for 10 min to suppress endogenous peroxidase activity, reducing non-specific background staining. The sections were washed

twice again with PBS and incubated overnight at 4°C with primary antibodies against CD31 (1:50, Abcam Inc., Waltham, MA, USA) to detect EC and against α-smooth muscle actin (α-SMA, Sigma-Aldrich) to detect vascular smooth muscle cells formed during neovascularization.[41]

Subsequently, the sections were washed three times with PBS. Phycoerythrin-conjugated goat anti-rabbit secondary antibodies (Santa Cruz Biotechnology Inc., Santa Cruz, CA, USA) were added to visualize the primary antibodies. For nuclei staining, 4′,6-diamidino-2-phenylindole (Sigma-Aldrich) was used. The images were captured using an inverted fluorescence microscope (IX-71, Olympus, Tokyo, Japan). To determine whether the angiogenic ability of the diabetic mouse model decreased, wound sections were compared between normal ICR mice and diabetic ICR mice.

### Statistical analysis

All data are presented as the mean ± standard deviation. Statistical analysis was conducted using either SPSS 25.0 software (IBM Corp., Armonk, NY, USA) or GraphPad Prism 8 software (GraphPad Software Inc., San Diego, CA, USA). One-way analysis of variance and post hoc analysis were used to identify differences between groups. Significance levels were set at $*p < 0.05$, $**p < 0.01$, and $***p < 0.001$.

## Results

### Concentration optimization of LNP-PTD-BMP2

To determine the optimal concentration of LNP-PTD-BMP2, we treated mice with LNP-PTD-BMP2 loaded in GHs at concentrations of 0 (0.1% egg lecithin without PTD-BMP2), 0.4, or 4 $\mu g/cm^2$ (Figure 1). We discovered that the mice treated with 0.4 $\mu g/cm^2$ LNP-PTD-BMP2 exhibited significantly enhanced wound closure, while those treated with 4 $\mu g/cm^2$ LNP-PTD-BMP2 showed no significant wound closure compared to the defect group (Figure 1(a) and (b)). Similar results were observed in the neovascularization study (Figure 1(c)). All samples were tested in triplicate.

Consequently, we subdivided the concentrations into 0, 25, 100, and 400 $ng/cm^2$ and obtained the wound healing capacity and neovascularization results (Figure 2). The groups treated with 100 and 400 $ng/cm^2$ LNP-PTD-BMP2 demonstrated significantly enhanced wound closure and collagen deposition compared to the defect, GH, and lower concentrations groups (Figure 2(a), (b), (e) and (f)). Comparing the neovascularization capacity of different concentrations in an immunofluorescence study revealed that the groups treated with 100 and 400 $ng/cm^2$ LNP-PTD-BMP2 displayed significantly higher numbers of CD31-positive cells than the defect, GH, and lower

concentrations groups (Figure 2(c) and (d)). Although a significantly higher number of CD31-positive cells was observed at the 400 $ng/cm^2$ concentration compared to the 100 $ng/cm^2$ concentration, mild wound inflammation was also detected. Therefore, we selected 100 $ng/cm^2$ as the optimal LNP-PTD-BMP2 concentration.

### Cell migration, cell proliferation, and angiogenesis study of LNP-PTD-BMP2 in vitro

A scratch cell migration assay on HaCaT cells was conducted to evaluate the efficacy of LNP-PTD-BMP2 in inducing in vitro cell migration compared to rhBMP2 (Figure 3(a)). HaCaT cells treated with LNP-PTD-BMP2 demonstrated a significantly enhanced cell migration capacity compared to those treated with the control and rhBMP2, exhibiting 81.3% wound gap closure at 48 h (Figure 3(b)).

To determine the effect of LNP-PTD-BMP2 on the proliferative capacity of HaCaT cells, the WST assay was performed (Figure 3(c)). HaCaT cells treated with LNP-PTD-BMP2 showed no significant differences in proliferative capacity compared to the control group, suggesting that LNP-PTD-BMP2 does not inhibit the growth of HaCaT cells.

HUVEC capillary tube formation assays were conducted to assess LNP-PTD-BMP2-induced angiogenesis in vitro (Figure 3(d)). To mimic an environment with oxidative stress similar to the diabetic environment,[42] we added $H_2O_2$ to the cells. Images were obtained after 6 h and quantified. Compared to the control and rhBMP2 treatments, LNP-PTD-BMP2 treatment displayed significantly higher tube and node formation capacity (Figure 3(e)). Intracellular transduction efficiency of LNP-PTD-BMP2 was confirmed by western blot analysis (Figure 3(f)).

### In vivo BMP2 release profile of LNP-PTD-BMP2-loaded GH

ICG labeling was utilized to investigate the in vivo BMP2 release profile of rhBMP2- or LNP-PTD-BMP2-loaded GH. In vivo near-infrared fluorescent images acquired are displayed in Figure 4(a). Wounds treated with LNP-PTD-BMP2-loaded GH exhibited high fluorescent intensity until day 7 (Figure 4(b)). The fluorescent intensity of wounds treated with rhBMP2-loaded GH significantly diminished from day 5 onward. Consequently, LNP-PTD-BMP2 demonstrated a longer half-life than rhBMP2.

### Wound closure and histological changes of LNP-PTD-BMP2 in diabetic wound healing

We confirmed the decreased wound healing capacity in an STZ-induced diabetic mouse model used to simulate Type
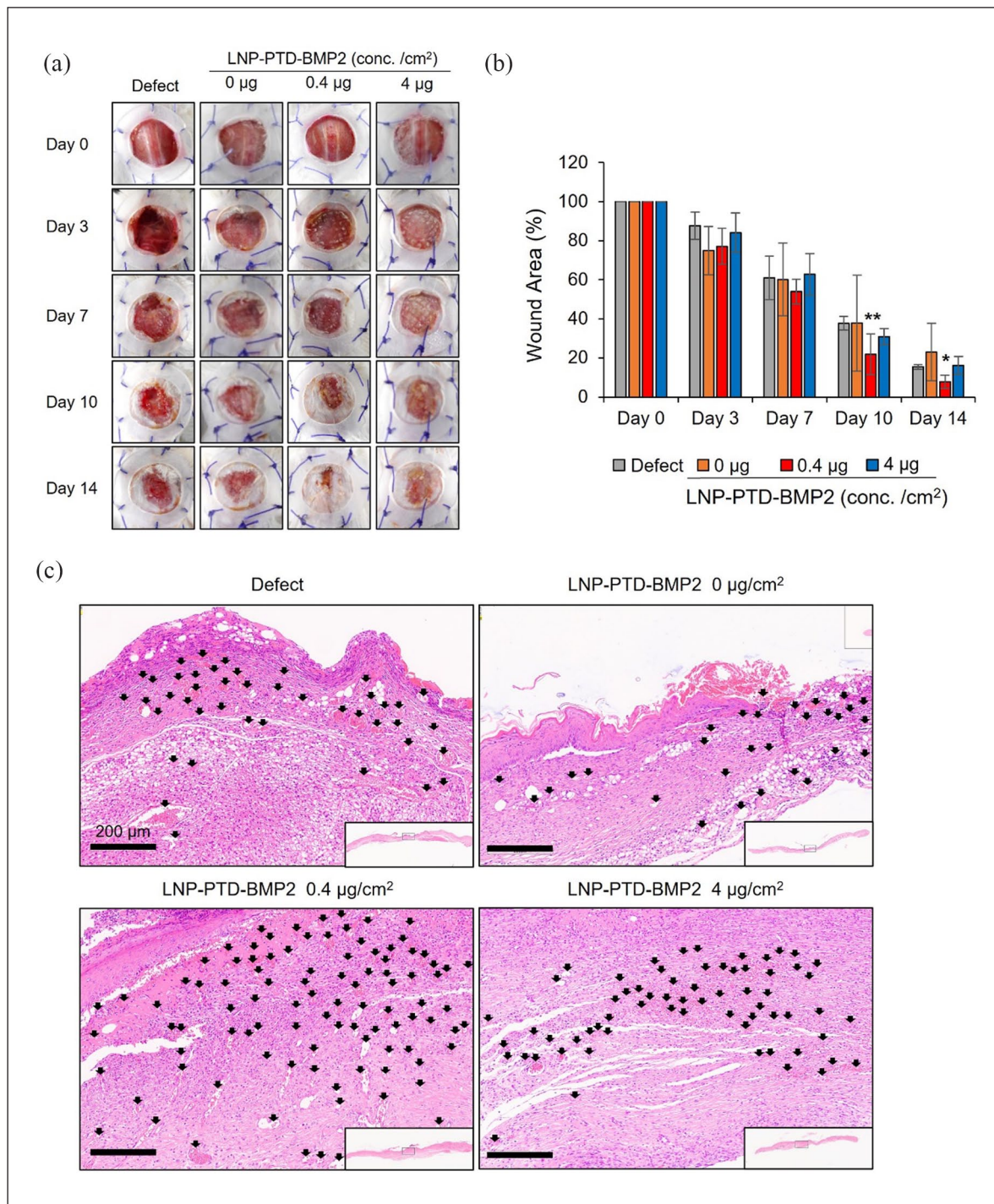
**Figure 1.** Optimization of LNP-PTD-BMP2 concentration (1). (a) Large full-thickness back skin wounds were inflicted on streptozotocin-induced diabetic mice and treated with LNP-PTD-BMP2-loaded GH at concentrations of 0, 0.4, and 4 μg/cm². Photographs of the wounds were taken on days 0, 3, 7, 10, and 14. (b) Quantitative analysis of wound closure rates for each concentration. (c) Hematoxylin and eosin-stained microscopic images of newly formed red capillary vasculature (black arrows) in the regenerated tissue for each concentration on day 14.

1 diabetes (Supplemental Figures S1A, S1B).[43] We also investigated the effect of rhBMP2 or LNP-PTD-BMP2-loaded GH on wound closure in this model (Figure 5(a) and (b)). The LNP-PTD-BMP2 group exhibited significantly enhanced regeneration capacity compared to the GH group after day 3. When compared to the rhBMP2
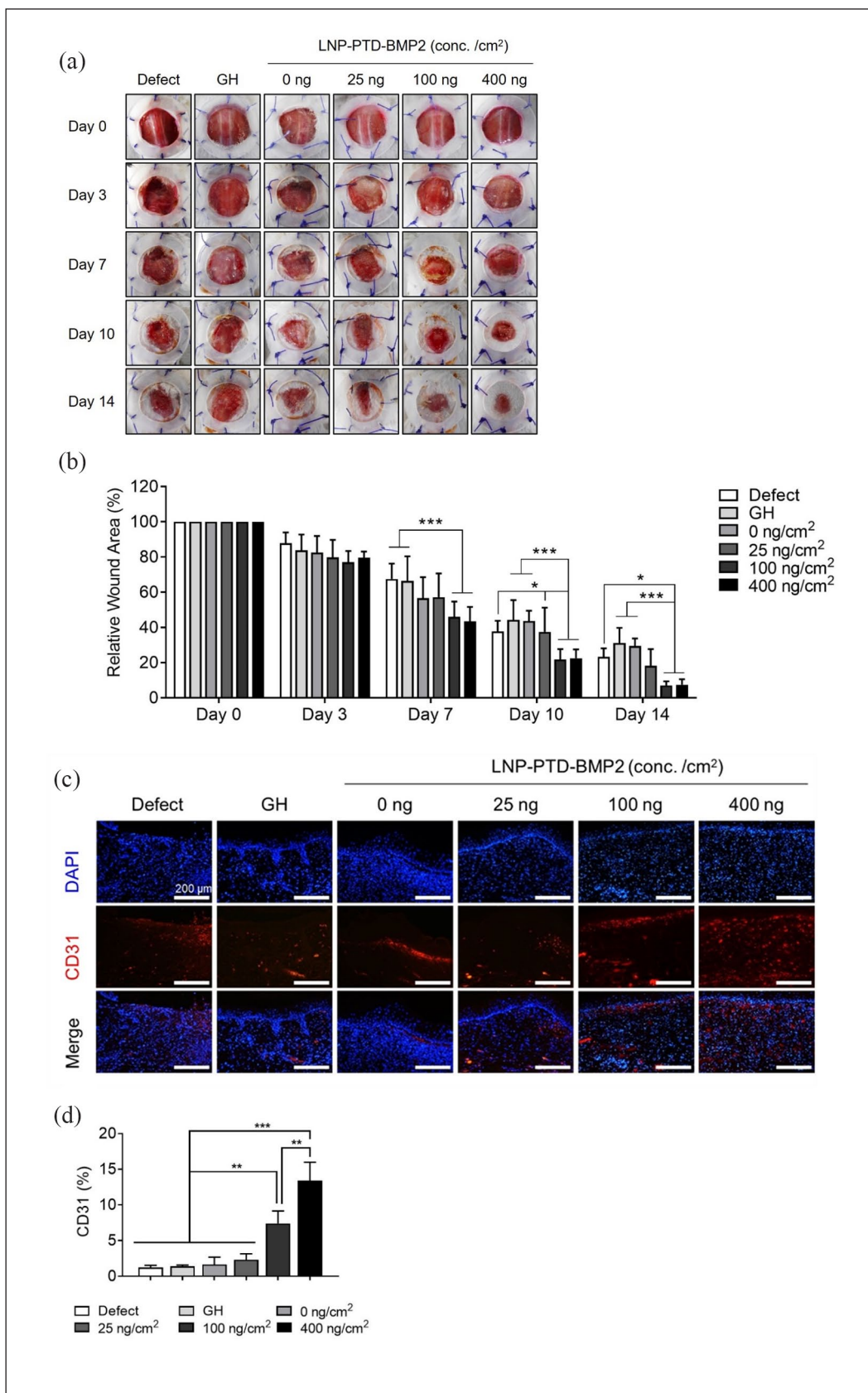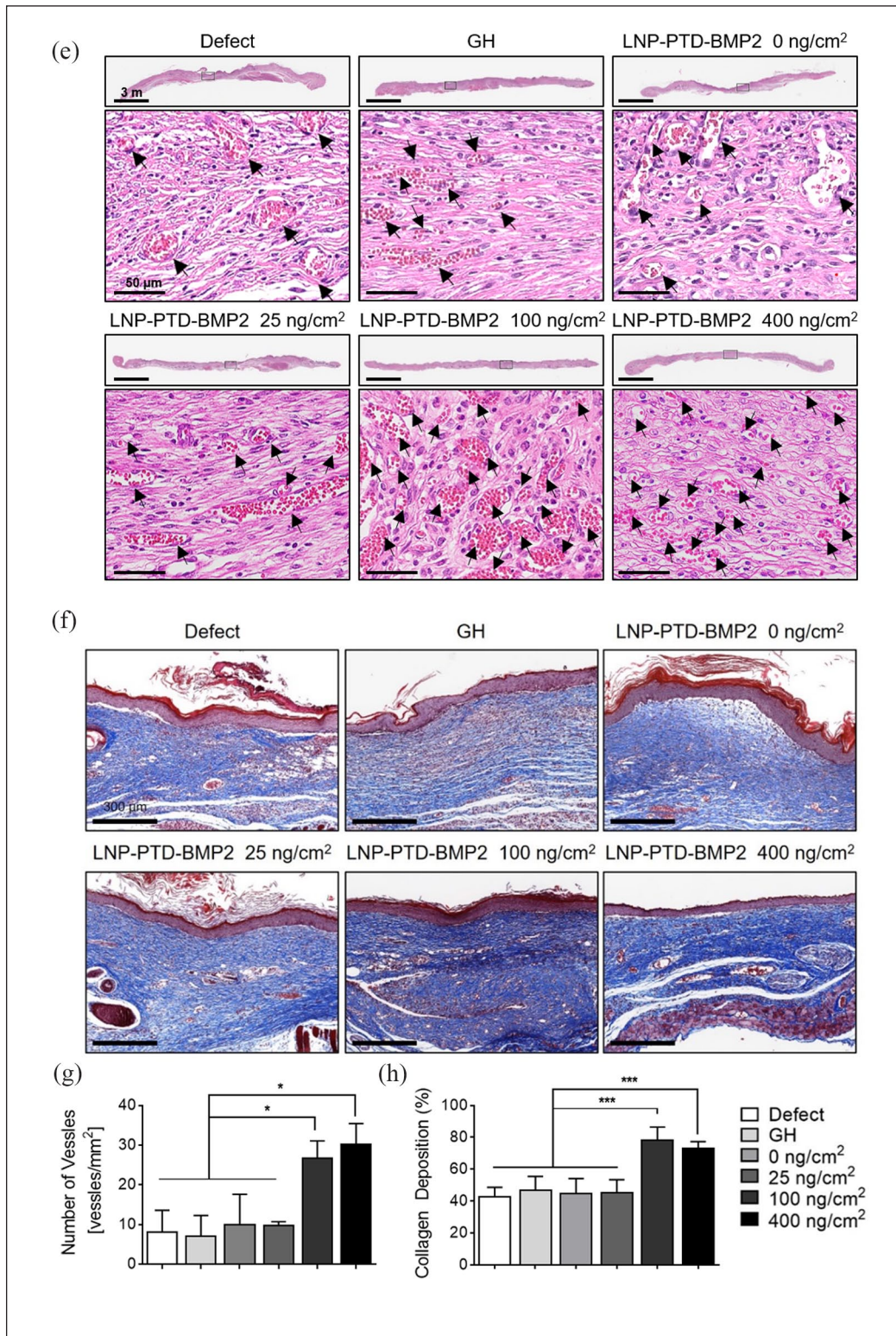
**Figure 2.** *(Continued)*

**Figure 2.** Optimization of LNP-PTD-BMP2 concentration (2). (a) Large full-thickness back skin wounds created in streptozotocin-induced diabetic mice were treated with gelatin hydrogel (GH) and LNP-PTD-BMP2-loaded GH at concentrations of 0, 25, 100, and 400 ng/cm$^2$. Representative images depict the skin wounds on days 0, 3, 7, 10, and 14. (b) Quantitative analysis of wound healing rate relative to the initial wound over time. (c) Immunofluorescence staining reveals CD31 expression in regenerated wound tissues on day 14. (d) Quantitative analysis of CD31-positive cells. (e) Hematoxylin and eosin-stained microscopic images of newly formed red capillary vasculature (black arrows) in the regenerated tissue at concentrations of 0, 25, 100, and 400 ng/cm$^2$ on day 14. (f) Masson's Trichrome-stained regenerated soft tissues on day 14. Granulation tissue displays the deposition of newly formed collagen tissues (blue areas). (g) Enumeration of the newly formed red capillary vasculature. (h) Quantitative analysis of collagen deposition for each concentration. All quantitative analyses were performed using ImageJ software.
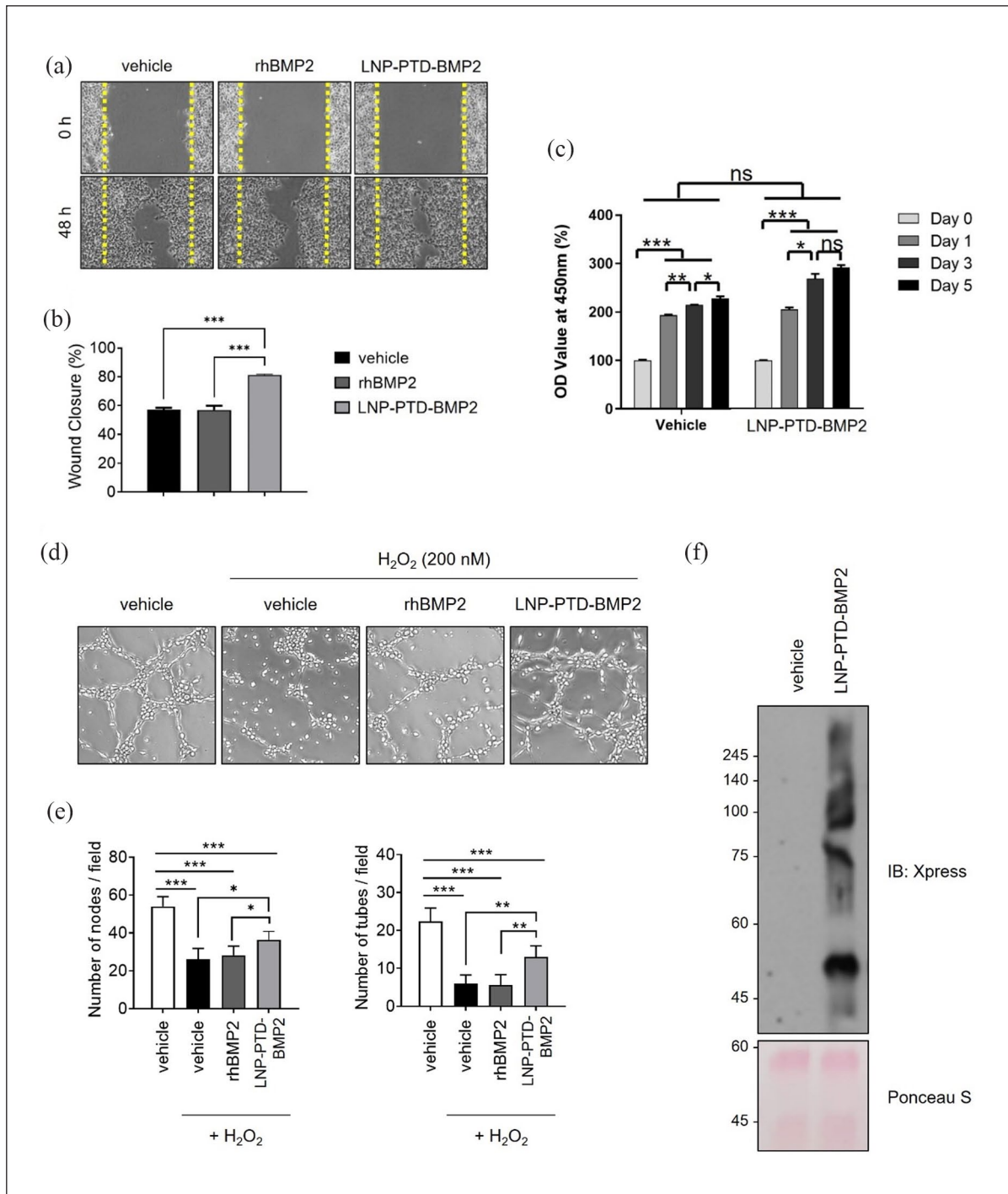
**Figure 3.** LNP-PTD-BMP2 enhanced migration and angiogenesis in vitro. (a) Incubated HaCaT cells ($2 \times 10^5$ cells/mL) were scratched and treated with rhBMP2 (100 ng/mL) or LNP-PTD-BMP2 (100 ng/mL). After 48 h of culture, gap differences were measured from the initial time point. (b) Wound closure rates were quantified using ImageJ software. (c) A water-soluble tetrazolium salt assay was performed to determine the proliferative capacity of LNP-PTD-BMP2-treated HaCaT cells. Each experiment was conducted in triplicate ($n = 3$). All error bars indicate $\pm$ SEM. (d) HUVECs were treated with vehicle, $H_2O_2$ combined with vehicle, $H_2O_2$ combined with rhBMP2 (100 ng), or $H_2O_2$ combined with LNP-PTD-BMP2 (100 ng) for tube formation assays. Representative images were taken after 6 h. (e) The number of nodes and tubes were quantified. Results from five independent experiments are presented. (f) HUVECs were treated with 500 ng of LNP-PTD-BMP2 overnight, and the insoluble fraction was used for western blotting.
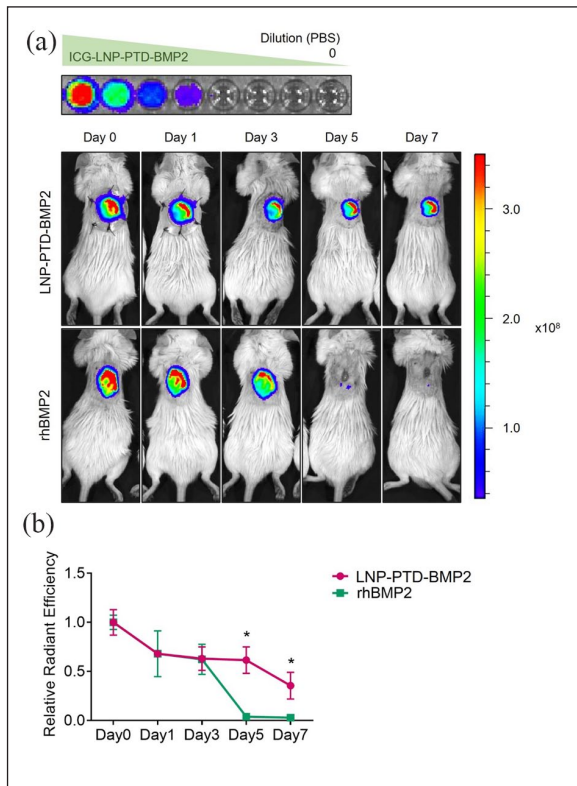
**Figure 4.** In vivo BMP2 release profile of rhBMP2- or LNP-PTD-BMP2-loaded gelatin hydrogel (GH) using indocyanine green (ICG) labeling. (a) ICG signal from the back wounds was observed using IVIS at 1, 3, 5, and 7 days after treating streptozotocin-induced diabetic mice with ICG-labeled rhBMP2- or LNP-PTD-BMP2-loaded GH. Wounds treated with LNP-PTD-BMP2-loaded GH maintained high fluorescence intensity until day 7, while wounds treated with rhBMP2-loaded GH showed an abrupt decrease in intensity from day 5 onward. (b) The relationship of the relative radiant efficiency of ICG-labeled LNP-PTD-BMP2 and rhBMP2 revealed that LNP-PTD-BMP2 has a longer half-life than rhBMP2.

group, the LNP-PTD-BMP2 group demonstrated a significantly reduced wound size after day 7. No significant difference in wound healing over time was observed between the rhBMP2 and GH groups.

To investigate re-epithelialization rates and collagen deposition, we analyzed the regenerated skin tissues using H&E and MT staining on day 14. The epithelial layer of wound sites treated with LNP-PTD-BMP2-loaded GH exhibited the best re-epithelialization rate (Figure 5(c) and (d)). The rhBMP2 group displayed a re-epithelialization rate similar to the GH group ($p = 0.779$). The LNP-PTD-BMP2 group showed significantly higher collagen deposition than the GH (3.3-fold) and rhBMP2 groups (4.1-fold), respectively (Figure 5(e) and (f)).

To assess whether BMP2 induces calcification of wounds and regenerated tissue, we analyzed regenerated skin perilesional tissues using Von Kossa staining on day

14. No calcium deposits were observed in the regenerated tissues of all groups (Supplemental Figure S2).

## Neovascularization of LNP-PTD-BMP2 in diabetic wound healing

To assess wound neovascularization, we used H&E staining, as well as CD31 and α-SMA immunofluorescence labeling. The number of red capillary vasculatures stained with H&E was significantly higher in the LNP-PTD-BMP2 group than in the GH or rhBMP2 group (Figure 6(a) and (b)). The numbers of CD31-positive cells and α-SMA-positive cells were significantly greater in the regenerated tissue of the LNP-PTD-BMP2 group than in the GH or rhBMP2 group (Figure 6(c) and (d)). The rate of CD31-positive cells in the LNP-PTD-BMP2 group was 1.7- and 1.8-fold higher than the rates in the GH and rhBMP2 groups, respectively. Similarly, the rate of α-SMA-positive cells was found to be 2.9- and 3.1-fold higher, respectively.

## Discussion

Angiogenic capacity is decreased in diabetic chronic wounds and plays a critical role in the pathogenesis of impaired wound healing.[6,7] Various studies have been conducted to identify treatments that improve angiogenesis in chronic wounds.[41,44] Previous therapeutic approaches have used growth factors, endothelial progenitor cells, and stem cells, but the results have been limited.[45–48]

BMP was the first member of the TGF-beta superfamily known to induce bone formation.[49] rhBMP2 has been widely used for spinal fusion in orthopedic surgery. It has shown promising results, but complications were reported in studies using high doses; 9.9% of patients who underwent anterior cervical fusion and used a high dose of rhBMP2 developed a hematoma after surgery.[50–52] Among them, 73.3% developed a hematoma 4–5 days after surgery.[50] Hematomas correlated with a high dose of rhBMP2 showed a higher frequency and later onset than other hematomas that occurred in patients who underwent anterior cervical fusion without rhBMP2.[50] This report led to the idea that BMP2 may also be involved in angiogenesis.

BMP2 plays an essential role in pathobiological processes and the homeostasis of skin and various tissues.[53] It induces chemotaxis in microvascular ECs.[45,54] BMP2 receptor mutations were identified in 70% of patients with familial pulmonary arterial hypertension, which is an uncommon vascular disorder.[55–57] Decreased expression of BMP2 receptors in lung tissues leads to EC dysfunction, resulting in increased vascular resistance.[13,55,58,59] In fetal skin, BMP2 promotes dermal and epidermal growth and appears to be involved in wound healing.[60] Therefore,
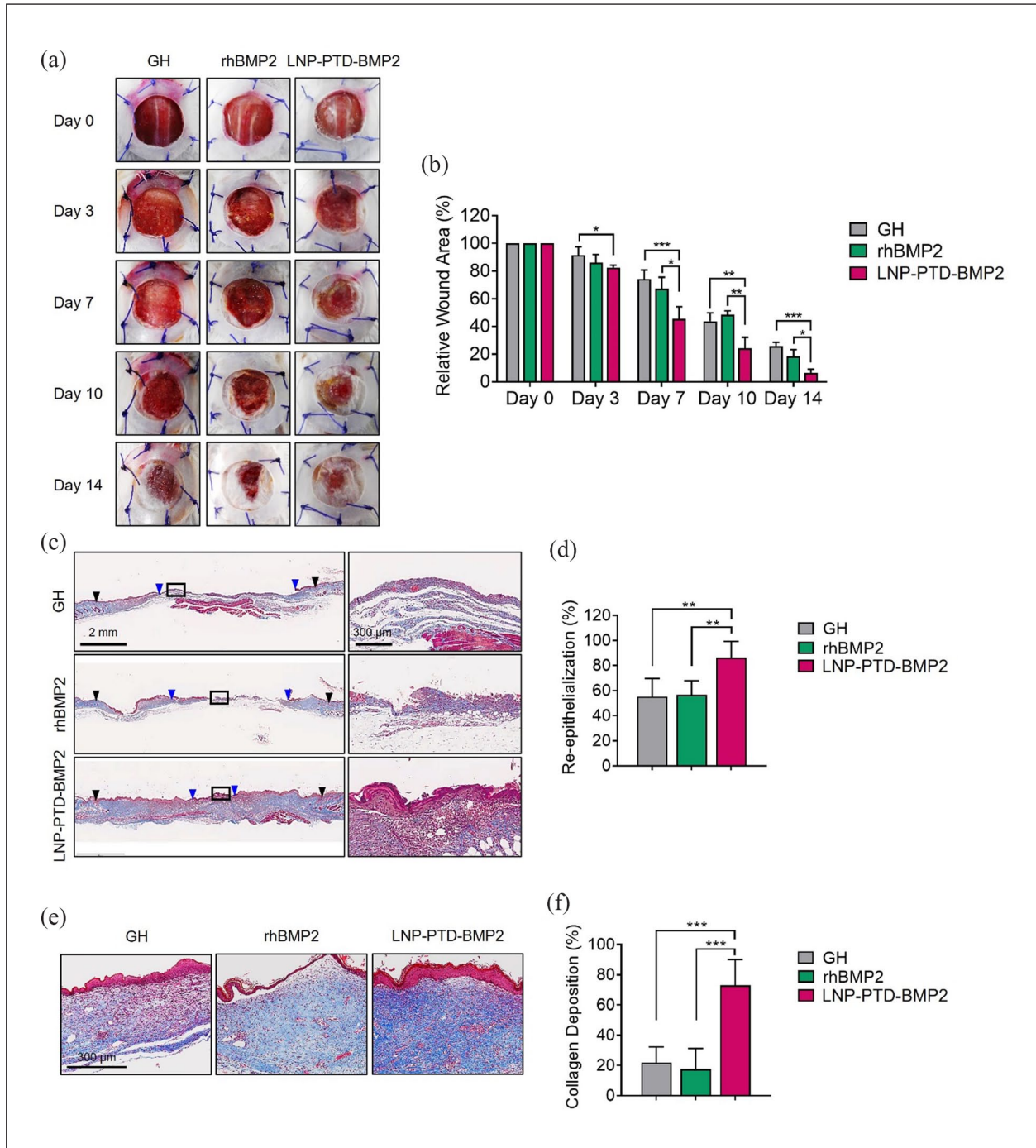
**Figure 5.** Comparisons of wound closures and histological changes between rhBMP2- and LNP-PTD-BMP2-loaded gelatin hydrogel (GH) in diabetic wound healing. (a) Wound healing effects of rhBMP2- and LNP-PTD-BMP2-loaded GH in the streptozotocin-induced diabetic mice. rhBMP2 (100 ng/cm$^2$)- and LNP-PTD-BMP2 (100 ng/cm$^2$)-loaded GHs were applied to the back wounds. Photographs of wounds were taken on days 0, 3, 7, 10, and 14. (b) Quantitative analysis of the wound healing rate relative to the initial wound over time. (c) Masson's Trichrome (MT)-stained microscopic images were obtained on day 14 to assess the re-epithelialization rate. Black boxes indicate the portion of the remaining wounds. Black arrowheads indicate the ends of the initial wound. Blue arrowheads indicate the ends of the regenerated keratinocyte cell layer. (d) Quantitative analysis of the re-epithelialization rate. (e) Regenerated soft tissues were stained with MT, and microscopic images were obtained on day 14. MT-positive blue areas of granulation tissue indicate the deposition of newly formed collagen tissues. (f) Quantitative analysis of collagen deposition using ImageJ software.
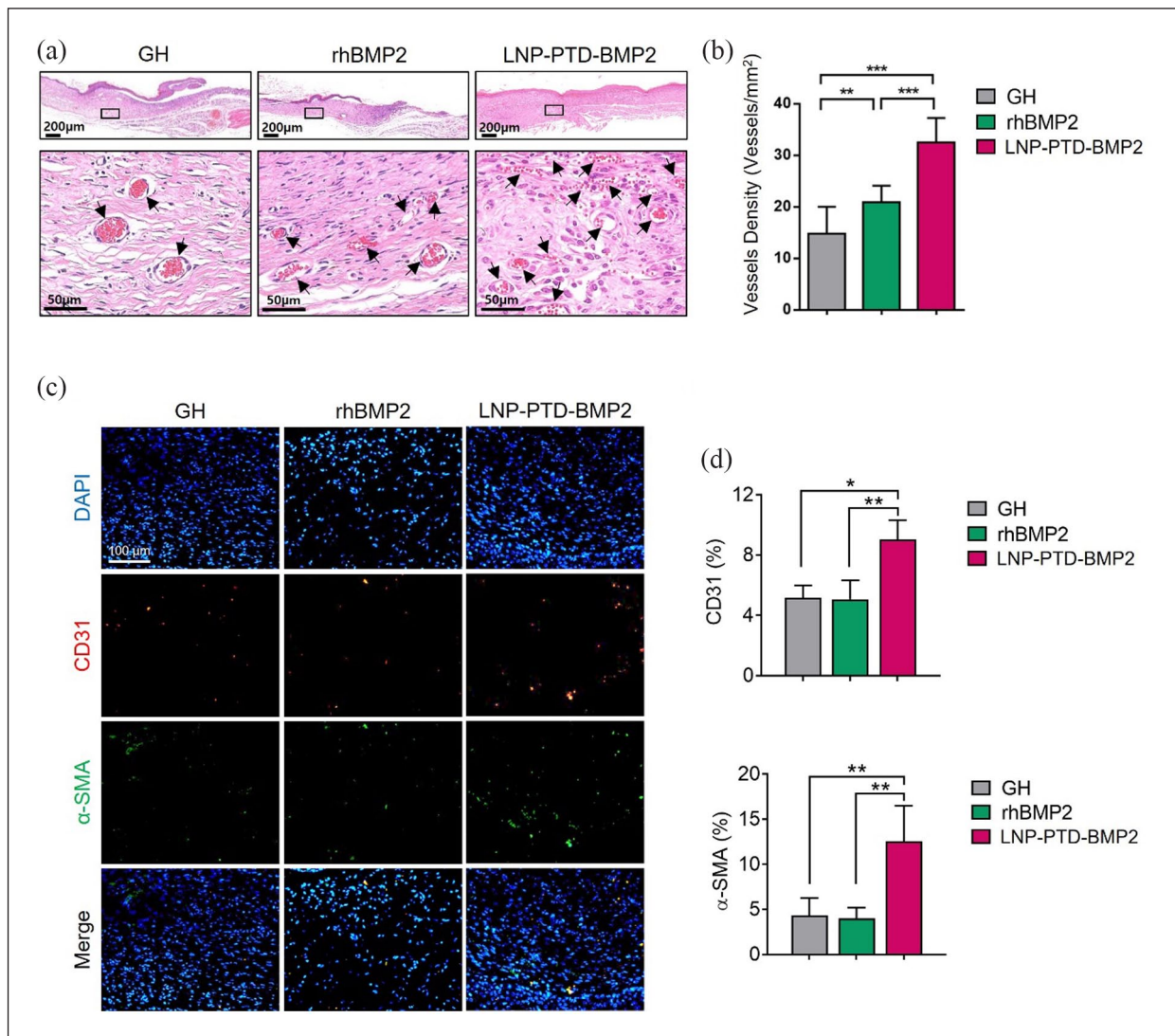
**Figure 6.** Neovascularization effects of rhBMP2- and LNP-PTD-BMP2-loaded gelatin hydrogel in streptozotocin-induced diabetic mice on day 14. (a) Microscopic images show newly formed red capillary vasculature (indicated by black arrows) in regenerated tissue obtained using hematoxylin and eosin staining. (b) Enumeration of the newly formed red capillary vasculature. (c) Immunofluorescence study demonstrates CD31-positive cells (red) and α-SMA-positive cells (green) in the regenerative tissue, suggesting the formation of mature vessels. (d) Quantitative analysis of CD31- and α-SMA-positive cells using ImageJ software.

treatment with BMP2 could be an ideal therapy for diabetic wound healing. The present study demonstrates the angiogenic and wound healing capacity of BMP2 in vitro and in vivo.

Previous studies have shown that BMP regulates the proliferation, migration, and tube formation of ECs.[21] BMP2 is known to exhibit various activities depending on the cell type. It stimulates the proliferation of human aortic ECs but does not affect the proliferation of HUVECs or human dermal microvascular ECs.[13,21] It also induces migration and tube formation in human aortic ECs, HUVECs, and human dermal microvascular ECs.[13] In this study, vessel formation was thought to be induced via the microvascular endothelial cells around the wound in vivo.

BMP2 is thought to be involved in angiogenesis during the possible mechanism by which it promotes wound healing. More research is needed to elucidate the specific mechanism underlying the effect of BMP2 on dermal and epidermal growth.

However, rhBMP2 is challenging to use for wound healing due to limitations such as a short half-life.[11,61] To overcome this limitation, we employed a novel delivery method using PTD formulated in micelles. In a previous study, micellized PTD-BMP7 was transduced directly into cells via an endosomal pathway, and active BMP7 was successfully secreted in HEK293 cells.[28] In our study, LNP-PTD-BMP2 was successfully delivered into cells independently of the BMP2 receptor to secrete active

BMP2 (Figure 3(f)). In another study, PTD-BMP7 injected intraperitoneally in Balb/C nude mice demonstrated a five times longer half-life and nine times greater area under the curve than rBMP7 in intravital fluorescence imaging.[26] Our study revealed that LNP-PTD-BMP2 has a longer half-life and duration of effect compared to rhBMP2 (Figure 4). Furthermore, when LNP-PTD-BMP2 was loaded into a GH and applied topically, LNP-PTD-BMP2 localized around the wound without a systemic effect, as shown in the in vivo BMP2 release study (Figure 4).

When using the PTD-mediated delivery method, the isolated and purified protein has the advantage of not exhibiting toxicity even at microgram concentrations in vitro, as reported in previously published papers.[11] Considering that a significant amount of protein permeates adjacent cells or tissues within minutes, it is expected that equivalent pharmacological effects can be expected when applied as a local treatment even when the protein is administered in a smaller amount than conventional soluble recombinant BMP.

Previous studies found that BMP2 promotes vascular calcification, resembling osteoblast differentiation in vessels.[23] In contrast, our study confirmed the absence of calcific deposits around the regenerative tissue using Von Kossa staining (Supplemental Figure S2). Based on the BMP2 release profile from the GH, this effect was observed locally around the wound without any systemic effect (Figure 4(a)).

In addition, possible adverse effects of BMP2 include inflammatory reactions in soft tissue and the risk of cancer development. In previous studies, soft tissue inflammation and swelling occurred at the surgical site as an adverse effect when BMP2 was administered in spinal fusion.[62,63] Considering that BMP2 is a chemoattractant of lymphocytes, monocytes, and macrophages, an inflammatory response is possible.[64] In this study, we observed more inflammation in the $0.4\,\mu g/cm^2$ LNP-PTD-BMP2 group than in the $0.1\,\mu g/cm^2$ group. Therefore, many inflammatory cells seem to be recruited during the wound-healing process. In an in vivo experiment using a rat femoral onlay model, when an absorbable collagen sponge loaded with a high concentration of BMP2 (4 mg/mL) was applied, a significant number of inflammatory cells were infiltrated and exudates were produced, compared to the control group.[64] The transfection and protein expression efficiency of LNP-PTD-BMP2 was good, indicating that sufficient BMP2 was produced even at $0.4\,\mu g/cm^2$, and more inflammation occurred at this concentration than at $0.1\,\mu g/cm^2$. Moreover, the risk of incidence of cancer was not high in retrospective cohort studies of spinal surgery and had no significant association with BMP2 use.[65,66] These adverse effects are thought to be caused by high concentrations of BMP2. LNP-PTD-BMP2, which was used in this study, can be used at a low dose and thus reduce adverse effects.

Meanwhile, Lewis et al. demonstrated that BMP signaling inhibits keratinocyte proliferation and migration in skin epithelium during wound healing.[67] In another study, BMP2 and BMP-4 negatively affected keratinocyte proliferation.[67–69] Different experimental settings or the half-life of BMP2 constructs may have influenced the results. Our study found that low concentrations of *E. coli*-derived rhBMP2 did not affect keratinocyte migration,[63,70,71] whereas the same concentration of LNP-PTD-BMP2 enhanced keratinocyte migration and did not inhibit proliferation in vitro (Figure 3(a)–(c)). In the group treated with LNP-PTD-BMP2, the continuous intracellular production of BMP2 protein was considered high. In addition, because rhBMP2 derived from *E. coli* was used at a low dose (100 ng/mL), it is thought that the effect was insignificant in this study. Furthermore, in our experimental settings with LNP-PTD-BMP2, we observed the activities of fibroblasts, ECs, and keratinocytes both in vitro and in vivo in the wound healing process of normal and diabetic mice. We used BMP2 in its active form after transduction, and angiogenesis and migration were improved and more prolonged, which may affect wound healing.

Our study demonstrates that BMP2 treatment enhances angiogenesis and diabetic wound healing. Previously, topical growth factor therapy, such as vascular endothelial growth factor (VEGF), exhibited limited success in diabetic foot wounds.[44] Although VEGF has demonstrated some angiogenic capacity, clinical trials have not shown significant effects, leading to unsuccessful treatments in clinical settings.[7,44] Several factors, including a short half-life, may have acted as limiting factors hindering its use in wound treatment. VEGF primarily acts on ECs and activates angiogenesis.[16] In contrast, BMP2 promotes activation and maturation of angiogenesis, affecting not only ECs but also vascular smooth muscle cells.[16] Additionally, BMP2 stimulates dermal and epidermal growth, resulting in keratinized and thickened skin.[45,60,72] Considering these factors, since BMP2 acts on various cells necessary for wound healing, we propose it as an excellent candidate for treating chronic wounds. As BMP2 is already used to induce bone formation clinically, its clinical application is extremely likely to expand following additional research on wound healing efficacy.

This study had several limitations. Firstly, the study subjects were limited to type 1 diabetes. Secondly, the long-term side effects of BMP2 were not confirmed. However, since BMP2 has received FDA approval for clinical use, it is not expected to have fatal side effects. BMP2 is an essential molecule that induces vascular calcification by acting on vascular smooth muscle cells. As microvessels were observed around wounds, BMP2 treatment does not appear to be related to cardiovascular pathology. Nonetheless, for safety, the long-term effects of BMP2 on wound sites need to be evaluated and validated through in vivo studies.

## Conclusion

We developed LNP-PTD-BMP2, which has the ability to promote direct intracellular transduction and angiogenesis. Based on the accelerated wound healing effects of LNP-PTD-BMP2 observed in this study, we propose that LNP-PTD-BMP2 is a potential therapeutic agent for the treatment of diabetic wounds.

## Author contributions

JWS and K-ML designed the study, analyzed the data, and wrote the paper. K-ML, EAK, DSY, NHK, HSK, and KHP conducted in vitro and in vivo experiments. JIY and JWL designed the study, provided financial support, and interpreted the data for the paper.

## Declaration of conflicting interests

The author(s) declared the following potential conflicts of interest with respect to the research, authorship, and/or publication of this article: J.I.Y. is an inventor of the patent related to this work filed by MET Life Sciences Co., Ltd. (Korean Patent Number: 10-2227966, PCT Application Number: PCT/KR2020/007011). N.H.K., H.S.K., and J.I.Y. are the founders of MET Life Sciences Co., Ltd. and shareholders. All other authors declare that they have no competing interests.

## ORCID iDs

Jae Wan Suh https://orcid.org/0000-0001-9386-6484
Kwang Hwan Park https://orcid.org/0000-0002-2110-0559

## Supplemental material

Supplemental material for this article is available online.

## References

1. Wang X, Sng MK, Foo S, et al. Early controlled release of peroxisome proliferator-activated receptor β/δ agonist GW501516 improves diabetic wound healing through redox modulation of wound microenvironment. *J Control Release* 2015; 197: 138–147.

2. Yoon DS, Lee Y, Ryu HA, et al. Cell recruiting chemokine-loaded sprayable gelatin hydrogel dressings for diabetic wound healing. *Acta Biomater* 2016; 38: 59–68.

3. Baltzis D, Eleftheriadou I and Veves A. Pathogenesis and treatment of impaired wound healing in diabetes mellitus: new insights. *Adv Ther* 2014; 31: 817–836.

4. Choi SM, Lee KM, Kim HJ, et al. Effects of structurally stabilized EGF and bFGF on wound healing in type I and type II diabetic mice. *Acta Biomater* 2018; 66: 325–334.

5. Singer AJ and Clark RA. Cutaneous wound healing. *N Engl J Med* 1999; 341: 738–746.

6. Xu J, Zgheib C, Hu J, et al. The role of microRNA-15b in the impaired angiogenesis in diabetic wounds. *Wound Repair Regen* 2014; 22: 671–677.

7. Okonkwo UA and DiPietro LA. Diabetes and wound angiogenesis. *Int J Mol Sci* 2017; 18: 1419. DOI: 10.3390/ijms18071419

8. Ridiandries A, Tan JTM and Bursill CA. The role of chemokines in wound healing. *Int J Mol Sci* 2018; 19: 3217. DOI: 10.3390/ijms19103217

9. Seo E, Lim JS, Jun JB, et al. Exendin-4 in combination with adipose-derived stem cells promotes angiogenesis and improves diabetic wound healing. *J Transl Med* 2017; 15: 35.

10. Galiano RD, Tepper OM, Pelo CR, et al. Topical vascular endothelial growth factor accelerates diabetic wound healing through increased angiogenesis and by mobilizing and recruiting bone marrow-derived cells. *Am J Pathol* 2004; 164: 1935–1947.

11. Kim NH, Cha YH, Kim HS, et al. A platform technique for growth factor delivery with novel mode of action. *Biomaterials* 2014; 35: 9888–9896.

12. Hong JY, Kim SH, Seo Y, et al. Self-assembling peptide gels promote angiogenesis and functional recovery after spinal cord injury in rats. *J Tissue Eng* 2022; 13: 20417314221086491.

13. Benn A, Haupt J, Hildebrandt S, et al. Physiological and pathological consequences of vascular BMP Signaling. In: Vukicevic S and Sampath KT (eds) *Bone morphogenetic proteins: Systems biology regulators*. Cham: Springer International Publishing, 2017, pp.367–407.

14. Das A and Botchwey E. Evaluation of angiogenesis and osteogenesis. *Tissue Eng Part B Rev* 2011; 17: 403–414.

15. Raida M, Clement JH, Leek RD, et al. Bone morphogenetic protein 2 (BMP-2) and induction of tumor angiogenesis. *J Cancer Res Clin Oncol* 2005; 131: 741–750.

16. David L, Feige JJ and Bailly S. Emerging role of bone morphogenetic proteins in angiogenesis. *Cytokine Growth Factor Rev* 2009; 20: 203–212.

17. Yoo SY and Kwon SM. Angiogenesis and its therapeutic opportunities. *Mediators Inflamm* 2013; 2013: 127170.

18. de Jesus Perez VA, Alastalo T-P, Wu JC, et al. Bone morphogenetic protein 2 induces pulmonary angiogenesis via Wnt–β-catenin and Wnt–RhoA–Rac1 pathways. *J Cell Biol* 2009; 184: 83–99.

19. Langenfeld EM and Langenfeld J. Bone morphogenetic protein-2 stimulates angiogenesis in developing tumors. *Mol Cancer Res* 2004; 2: 141–149.

20. Rothhammer T, Bataille F, Spruss T, et al. Functional implication of BMP4 expression on angiogenesis in malignant melanoma. *Oncogene* 2007; 26: 4158–4170.

21. Finkenzeller G, Hager S and Stark GB. Effects of bone morphogenetic protein 2 on human umbilical vein endothelial cells. *Microvasc Res* 2012; 84: 81–85.

22. Woo EJ. Adverse events after recombinant human BMP2 in nonspinal orthopaedic procedures. *Clin Orthop Relat Res* 2013; 471: 1707–1711.

23. Evrard S, Delanaye P, Kamel S, et al. Vascular calcification: from pathophysiology to biomarkers. *Clin Chim Acta* 2015; 438: 401–414.

24. Peiffer BJ, Qi L, Ahmadi AR, et al. Activation of BMP signaling by FKBP12 ligands synergizes with inhibition of CXCR4 to accelerate wound healing. *Cell Chem Biol* 2019; 26: 652–661. e4.

25. Frankel AD and Pabo CO. Cellular uptake of the tat protein from human immunodeficiency virus. *Cell* 1988; 55: 1189–1193.

26. Kim S, Shin DH, Nam BY, et al. Newly designed protein transduction domain (PTD)-mediated BMP-7 is a potential therapeutic for peritoneal fibrosis. *J Cell Mol Med* 2020; 24: 13507–13522.

27. Schwarze SR, Ho A, Vocero-Akbani A, et al. In vivo protein transduction: delivery of a biologically active protein into the mouse. *Science* 1999; 285: 1569–1572.

28. Kim S, Jeong CH, Song SH, et al. Micellized protein transduction domain-bone morphogenetic protein-7 efficiently blocks renal fibrosis via inhibition of transforming growth factor-beta-mediated epithelial-mesenchymal transition. *Front Pharmacol* 2020; 11: 591275.

29. Cho K, Kim NH, Seo SH, et al. A micellized bone morphogenetic protein-7 prodrug ameliorates liver fibrosis by suppressing transforming growth factor-β signaling. *Am J Cancer Res* 2022; 12: 763–778.

30. Kang ML, Kim HS, You J, et al. Hydrogel cross-linking-programmed release of nitric oxide regulates source-dependent angiogenic behaviors of human mesenchymal stem cell. *Sci Adv* 2020; 6: eaay5413.

31. Yang G, Xiao Z, Ren X, et al. Enzymatically crosslinked gelatin hydrogel promotes the proliferation of adipose tissue-derived stromal cells. *PeerJ* 2016; 4: e2497.

32. Moreno-Bueno G, Peinado H, Molina P, et al. The morphological and molecular features of the epithelial-to-mesenchymal transition. *Nat Protoc* 2009; 4: 1591–1613.

33. Park YR, Sultan MT, Park HJ, et al. NF-κB signaling is key in the wound healing processes of silk fibroin. *Acta Biomater* 2018; 67: 183–195.

34. Guo S, Lok J, Liu Y, et al. Assays to examine endothelial cell migration, tube formation, and gene expression profiles. *Methods Mol Biol* 2014; 1135: 393–402.

35. Chung HW and Lim JB. High-mobility group box-1 contributes tumor angiogenesis under interleukin-8 mediation during gastric cancer progression. *Cancer Sci* 2017; 108: 1594–1601.

36. Kim CK, Choi YK, Lee H, et al. The farnesyltransferase inhibitor LB42708 suppresses vascular endothelial growth factor-induced angiogenesis by inhibiting ras-dependent mitogen-activated protein kinase and phosphatidylinositol 3-kinase/Akt signal pathways. *Mol Pharmacol* 2010; 78: 142–150.

37. Baek YY, Cho DH, Choe J, et al. Extracellular taurine induces angiogenesis by activating ERK-, Akt-, and FAK-dependent signal pathways. *Eur J Pharmacol* 2012; 674: 188–199.

38. Francescone RA III, Faibish M and Shao R. A Matrigel-based tube formation assay to assess the vasculogenic activity of tumor cells. *J Vis Exp* 2011; 55: 3040.

39. Deng Y, Han X, Yao Z, et al. PPARα agonist stimulated angiogenesis by improving endothelial precursor cell function via a NLRP3 inflammasome pathway. *Cell Physiol Biochem* 2017; 42: 2255–2266.

40. Kim J, Lee KM, Han SH, et al. Development of stabilized dual growth factor-loaded hyaluronate collagen dressing matrix. *J Tissue Eng* 2021; 12: 2041731421999750.

41. Gao X, Ma S, Xing X, et al. Microvessels derived from hiPSCs are a novel source for angiogenesis and tissue regeneration. *J Tissue Eng* 2022; 13: 20417314221143240.

42. Singh A, Kukreti R, Saso L, et al. Mechanistic insight into oxidative stress-triggered signaling pathways and type 2 diabetes. *Molecules* 2022; 27: 950. DOI: 10.3390/molecules27030950

43. Lee M, Han SH, Choi WJ, et al. Hyaluronic acid dressing (Healoderm) in the treatment of diabetic foot ulcer: a prospective, randomized, placebo-controlled, single-center study. *Wound Repair Regen* 2016; 24: 581–588.

44. D'Amico R, Malucelli C, Uccelli A, et al. Therapeutic arteriogenesis by factor-decorated fibrin matrices promotes wound healing in diabetic mice. *J Tissue Eng* 2022; 13: 20417314221119615.

45. Moura J, da Silva L, Cruz MT, et al. Molecular and cellular mechanisms of bone morphogenetic proteins and activins in the skin: potential benefits for wound healing. *Arch Dermatol Res* 2013; 305: 557–569.

46. Sieveking DP and Ng MK. Cell therapies for therapeutic angiogenesis: back to the bench. *Vasc Med* 2009; 14: 153–166.

47. Kirana S, Stratmann B, Prante C, et al. Autologous stem cell therapy in the treatment of limb ischaemia induced chronic tissue ulcers of diabetic foot patients. *Int J Clin Pract* 2012; 66: 384–393.

48. Berlanga-Acosta J. Diabetic lower extremity wounds: the rationale for growth factors-based infiltration treatment. *Int Wound J* 2011; 8: 612–620.

49. Black C, Gibbs D, McEwan J, et al. Comparison of bone formation mediated by bone morphogenetic protein delivered by nanoclay gels with clinical techniques (autograft and InductOs®) in an ovine bone model. *J Tissue Eng* 2022; 13: 20417314221113746.

50. Shields LB, Raque GH, Glassman SD, et al. Adverse effects associated with high-dose recombinant human bone morphogenetic protein-2 use in anterior cervical spine fusion. *Spine* 2006; 31: 542–547.

51. Perri B, Cooper M, Lauryssen C, et al. Adverse swelling associated with use of rh-BMP-2 in anterior cervical discectomy and fusion: a case study. *Spine J* 2007; 7: 235–239.

52. Tannoury CA and An HS. Complications with the use of bone morphogenetic protein 2 (BMP-2) in spine surgery. *Spine J* 2014; 14: 552–559.

53. Botchkarev VA. Bone morphogenetic proteins and their antagonists in skin and hair follicle biology. *J Investig Dermatol* 2003; 120: 36–47.

54. Li G, Cui Y, McIlmurray L, et al. RhBMP-2, rhVEGF(165), rhPTN and thrombin-related peptide, TP508 induce chemotaxis of human osteoblasts and microvascular endothelial cells. *J Orthop Res* 2005; 23: 680–685.

55. Machado RD, Aldred MA, James V, et al. Mutations of the TGF-β type II receptor BMPR2 in pulmonary arterial hypertension. *Hum Mutat* 2006; 27: 121–132.

56. Thomson JR, Machado RD, Pauciulo MW, et al. Sporadic primary pulmonary hypertension is associated with germline mutations of the gene encoding BMPR-II, a receptor member of the TGF-beta family. *J Med Genet* 2000; 37: 741–745.

57. Ma L and Chung WK. The genetic basis of pulmonary arterial hypertension. *Hum Genet* 2014; 133: 471–479.

58. Atkinson C, Stewart S, Upton PD, et al. Primary pulmonary hypertension is associated with reduced pulmonary vascular expression of type II bone morphogenetic protein receptor. *Circulation* 2002; 105: 1672–1678.

59. Morrell NW, Adnot S, Archer SL, et al. Cellular and molecular basis of pulmonary arterial hypertension. *J Am Coll Cardiol* 2009; 54: S20–S31.

60. Hwang EA, Lee HB and Tark KC. Comparison of bone morphogenetic protein receptors expression in the fetal and adult skin. *Yonsei Med J* 2001; 42: 581–586.

61. Lo KW, Ulery BD, Ashe KM, et al. Studies of bone morphogenetic protein-based surgical repair. *Adv Drug Deliv Rev* 2012; 64: 1277–1291.

62. Mroz TE, Wang JC, Hashimoto R, et al. Complications related to osteobiologics use in spine surgery: a systematic review. *Spine* 2010; 35: S86–104.

63. Cho JH, Lee JH, Yeom JS, et al. Efficacy of Escherichia coli-derived recombinant human bone morphogenetic protein-2 in posterolateral lumbar fusion: an open, active-controlled, randomized, multicenter trial. *Spine J* 2017; 17: 1866–1874.

64. Zara JN, Siu RK, Zhang X, et al. High doses of bone morphogenetic protein 2 induce structurally abnormal bone and inflammation in vivo. *Tissue Eng Part A* 2011; 17: 1389–1399.

65. Cooper GS and Kou TD. Risk of cancer after lumbar fusion surgery with recombinant human bone morphogenic protein-2 (rh-BMP-2). *Spine* 2013; 38: 1862–1868.

66. Malham GM, Giles GG, Milne RL, et al. Bone morphogenetic proteins in spinal surgery: what is the fusion rate and do they cause cancer? *Spine* 2015; 40: 1737–1742.

67. Lewis CJ, Mardaryev AN, Poterlowicz K, et al. Bone morphogenetic protein signaling suppresses wound-induced skin repair by inhibiting keratinocyte proliferation and migration. *J Invest Dermatol* 2014; 134: 827–837.

68. Ahmed MI, Mardaryev AN, Lewis CJ, et al. MicroRNA-21 is an important downstream component of BMP signalling in epidermal keratinocytes. *J Cell Sci* 2011; 124: 3399–3404.

69. Sharov AA, Sharova TY, Mardaryev AN, et al. Bone morphogenetic protein signaling regulates the size of hair follicles and modulates the expression of cell cycle-associated genes. *Proc Natl Acad Sci USA* 2006; 103: 18166–18171.

70. Kim NH, Jung SK, Lee J, et al. Modulation of osteogenic differentiation by Escherichia coli-derived recombinant bone morphogenetic protein-2. *AMB Express* 2022; 12: 106.

71. Kübler NR, Reuther JF, Faller G, et al. Inductive properties of recombinant human BMP-2 produced in a bacterial expression system. *Int J Oral Maxillofac Surg* 1998; 27: 305–309.

72. Francois S, Eder V, Belmokhtar K, et al. Synergistic effect of human bone morphogenic protein-2 and mesenchymal stromal cells on chronic wounds through hypoxia-inducible factor-1 alpha induction. *Sci Rep* 2017; 7: 4272.